REPORT DOCUMENTATION PAGE

Form Approved
OMB No. 0704-0188

1. REPORT DATE *(DD-MM-YYYY)*	2. REPORT TYPE	3. DATES COVERED *(From - To)*
01/14/2008	Final Report	05/01/2006-12/31/2006

4. TITLE AND SUBTITLE
Controlling Interfacial Properties in Nanoenvironments:
A Novel Technique of Intelligent Systems

5a. CONTRACT NUMBER
858-534-3388

5b. GRANT NUMBER
FA9550-06-0181

5c. PROGRAM ELEMENT NUMBER

6. AUTHOR(S)
Yu Qiao
Current Address: 9500 Gilman Dr., MC 0085, La Jolla, CA 92093-0085

5d. PROJECT NUMBER

5e. TASK NUMBER

5f. WORK UNIT NUMBER

7. PERFORMING ORGANIZATION NAME(S) AND ADDRESS(ES)
University of Akron
Akron, Ohio 44325-3905

8. PERFORMING ORGANIZATION REPORT NUMBER

9. SPONSORING / MONITORING AGENCY NAME(S) AND ADDRESS(ES)
Dr. Byung-Lip Lee
AFOSR
875 N Randolph St
Arlington, VA 22203

10. SPONSOR/MONITOR'S ACRONYM(S)

11. SPONSOR/MONITOR'S REPORT NUMBER(S)

12. DISTRIBUTION / AVAILABILITY STATEMENT
Approved for public release,
distribution unlimited

AFRL-SR-AR-TR-08-0129

13. SUPPLEMENTARY NOTES

14. ABSTRACT

In summary, it is validated experimentally that nanoporous materials of non-hysteretic sorption isotherm curves can be employed to develop volume memory systems. Under the working pressure, as temperature changes, the effective wettability varies, and thus the liquid tends to either infiltrate into or defiltrate out of the nanopores, resulting in a thermally controllable actuation behavior. Due to the large specific surface area, the wettability variation is greatly amplified. Consequently, the energy density can be much higher than that of conventional smart solids. In addition, through a controlled-temperature infiltration-defiltation experiment, it is validated that using electrolyte with temperature sensitive solubility can significantly increase the output energy density of nanoporous material functionalized liquids, providing a promising way to enhance their performance. The infiltration pressure does not vary monotonically with the temperature; rather, there exists a critical temperature at which the infiltration pressure reaches the maximum value, which can be attributed to the competition between the thermocapillary effect and the cation exchange effect. The former mechanism is dominant in the high-temperature range and the latter is more pronounced in the low-temperature range.

15. SUBJECT TERMS

16. SECURITY CLASSIFICATION OF:			17. LIMITATION OF ABSTRACT	18. NUMBER OF PAGES	19a. NAME OF RESPONSIBLE PERSON
a. REPORT	b. ABSTRACT	c. THIS PAGE		10	3
					19b. TELEPHONE NUMBER *(include area code)* 858-534-3388

Standard Form 298 (Rev. 8-98)
Prescribed by ANSI Std. Z39.18

FINAL REPORT FOR THE RESEARCH WORK AT UNIVERSITY OF AKRON FOR AFOSR GRANT NO. FA9550-06-1-0181

Grant No.: FA9550-06-1-0181
PI: Dr. Yu Qiao
Period of Performance: April 1st, 2006 – July 31st, 2006
Place of Operation: The University of Akron

Total Amount of the Three-Year Program: $346,674
Expenditures To-Date: $15,522
Un-Expended Amount: $331,152

Reason of Project Termination

From April 1st, 2006 to July 31st, 2006, The Air Force Office of Scientific Research supported Dr. Qiao's research on intelligent nanoporous systems under Grant No. FA9550-06-1-0181. This is the beginning period of a three-year program, and is terminated because the PI has left The University of Akron, the initial place of operation, and started to work at The University of California at San Diego. The PI will submit a proposal to continue the same research shortly. This transfer will not affect the proposed research and work plan.

Publications and Presentations Supported by The AFOSR

- Journal Publications

  Han, A. and Qiao, Y. Pressure induced infiltration of aqueous solutions of multiple promoters in a nanoporous silica. *J. Am. Chem. Soc.*, in the press.

  Surani, F. B. and Qiao, Y. Infiltration and defiltration of an electrolyte solution in nanopores. *J. Appl. Phys.*, in the press.

  Han, A., Kong, X., and Qiao, Y. Pressure induced liquid infiltration in nanopores. *J. Appl. Phys.* **100**, 014308.1-3 (2006).

- Conference Presentations

  Qiao, Y., Han, A., Surani, F. B. Using nanoporous material functionalized liquid in intelligent structures. *The 15th US National Congress of Theoretical and Applied Mechanics*, Boulder, Colorado (June 25-30, 2006)

Demographic Data

(a) Number of Manuscripts submitted during this reporting period: 4
(b) Number of Peer Reviewed Papers submitted during this reporting period: 4
(c) Number of Non-Peer Reviewed Papers submitted during this reporting period: 0
(d) Number of Presented but not Published Papers submitted during this reporting period: 1
(e) Number of Graduate Students: 2
(f) Number of Postdoc Associates: 1

Scientific Progress and Acomplishements

The pressure induced infiltration of nanoporous materials has recently received increasing attention. When hydrophobic nanoporous materials are immersed in water, at the atmosphere pressure, p_{at}, due to the capillary effect soaking does not occur spontaneously. As the pressure increases to a critical value, p_{in}, water can infiltrate into the nanopores, accompanied by a large increase in solid-liquid interfacial energy. When the pressure is reduced back to p_{at}, however, the water molecules may not come out of the nanoenvironment, depending on the factors that are still under investigation. According to the limited data currently available in open literature, the "nonoutflow" is likely to occur when the pore size is in the mesoporous range (2-80 nm), and the "outflow" is relatively easy if the pore size is smaller than about 1-2 nm.

The conventional interface and microfluidic theories, such as the Washburn type analyses in which the solid-liquid interfaces are assumed to be isolated, have failed in explaining this size effect, as well as the thermal effect, the recovery behavior, the dynamic behavior, the system selectivity, and the gas diffusion phenomenon that will be discussed shortly. In order to model the pressure induced infiltration, a few frameworks, such as the evolution of pore clusters, the flow-direction dependence of contact angle, and the phase transformation with constant system volume and zero gas-phase nucleation barrier, have been proposed. However, currently, since the experimental setups are usually sophisticated and the direct observation of infiltration processes is difficult, there are few experimental evidences that can support these theories. For instance, at the nm scale, the basis of continuum fluid mechanics involved in the effective phase transformation and the flow direction theory may no longer be valid, and ignoring the system volume change and the energy exchange between gas/liquid phases can be questionable.

We designed a simple transparent poly(methyl methacrylate) (PMMA) system so as to directly observe the infiltration/defiltration behaviors of nanoporous particles. The material under investigation was end-capped Fluka 100 C_8 reversed phase mesoporous silica with the average pore size $\bar{r}$ = 7.8 nm and the standard deviation δr = 2.4 nm. The specific pore volume was 560 mm^3/g, and the specific surface area was 287 m^2/g. The Barrett-Joyner-Halenda (BJH) adsorption characterization measurement was performed at the Quantachrome Instruments. The surface coverage was 10-12% ($\pm$ 4 $\mu mol/m^2$), which led to a high degree of hydrophobicity. The particle size was in the range of 15-35 μm. Prior to the infiltration tests, the silica particles had been heated in air at 150°C for 12 hours.

The aqueous suspension of 0.5 g of the mesoporous silica particles was sealed in the PMMA cylinder by a stainless steel piston with reinforced gaskets. Initially, no air bubble could be observed. The infiltration experiment was performed using an Instron 5569 machine. The piston was first compressed into the container at a constant rate of 1.0 mm/min. Once the pressure exceeded about 50 MPa, the crosshead was moved back at the same speed. The loading-unloading cycle was repeated until the absorption isotherm curves converged to the steady-state, as shown by curves (a, b) in Fig.1, where the specific volume variation is defined as $\Delta V_0/W$, with ΔV_0 being the volume change of the system and W the mass of the silica gel. The system was then thermally treated in a temperature bath in the range of 30-80°C for 0.5 hour either (1) immediately or (2) after resting at room temperature for 6-24 hours, followed by another loading-unloading test. The testing results are shown by curves (c, d) in Fig.1, respectively. Altogether four samples were tested.

Curve (a) in Fig. 1 shows that, following the initial linear stage, as the pressure reached the infiltration pressure, $p_{in} \approx$ 17 MPa, the water was forced into the nanopores, causing the large increase in system compressibility. If the pore size were perfectly uniform, the plateau should be flat. In the current system, due to the pore size distribution, the slope of the absorption isotherm was finite. Eventually, at about 30 MPa, most of the pores were filled and the system compressibility decreased rapidly. The volume variation associated with the plateau region was about 0.55 cm^3/g, close to the BJH result of the specific pore volume. As the pressure was reduced, the confined water remained in the nanopores, and thus the unloading curves were quite linear. During the loading-unloading process, there was no significant change in system appearance, except for the variation in volume, indicating that the gas entrapped in the nanopores dissolved in the liquid phase. Since no air bubble could be observed even when the pressure was reduced back to the atmosphere pressure, the gas content in the liquid phase outside the nanoporous particles must be quite constant; that is, the gas molecules remained in the nanopores. Because of the "nonoutflow", the extent of infiltration was considerably lowered in the following loading-unloading cycles (see curve b in Fig.1).

When, immediately after the first loading-unloading cycle, the system was thermally treated, the liquid phase was still clear and little air bubbles were formed. However, the energy absorption capacity of the system was recovered significantly (see curve c in Fig.1 and Table I), indicating clearly that after the thermal treatment a certain portion of the porous space was occupied by gas phase. When the temperature exceeded 50°C, the system could be almost fully recovered.

If, on the other hand, after the first infiltration cycle, the specimen was rested at room temperature under p_{at}, the system appearance would change gradually. After 6 hours, a large number of air bubbles with the sizes in the range of 0.05 mm to 0.5 mm were formed and therefore the sample was no longer transparent. After 24 hours, the total volume of the air bubbles was estimated as 0.25 cm^3/g, while the energy absorption capacity was still close to zero, suggesting that the nanopores were still filled by liquid. Thermally treating this system would cause a partial recovery, as shown by curve (d) in Fig.1, where the system recoverability, R_p, is defined as $\dot{E}_t/\dot{E}_1$, with $\dot{E}_t$ being the absorbed energy in the loading-unloading cycle subsequent to the postponed thermal treatment; the treatment temperature was set to 70°C; and t_r is the room-temperature resting time. Clearly, during the room-temperature resting, a certain amount of gas molecules diffused out of the nanopores, and the decrease in system recoverability should be attributed to the reduced excess gas content in the nanoenvironment.

The motion of the gas-liquid contact line in a nanopore can be considered as the result of expansion or shrinkage of the gas phase. Note that at the nm level, sharp liquid-gas interfaces may not exist. Nevertheless, effective boundaries can be defined, e.g. in the context of Gibbs dividing surfaces, as shown in Fig.2. In an initially filled nanopore, the formation of a gas phase nucleus increases the free energy of system by (a) $\Delta\mu \cdot V_G$, where $\Delta\mu$ is the specific nucleation energy and $V_G = \pi r^2 h$ is the volume of the gas phase, with h being the nucleus length; (b) $\gamma_{GL} \cdot A_{GL}$, where γ_{GL} is the surface tension of the liquid and $A_{GL} = 2\pi r^2$ is the gas-liquid interface area; and (c) the external work $p \cdot \Delta V$, where p is the applied pressure and $\Delta V = V_G$ is the system volume change. On the other hand, with the nucleation of the gas phase, since the liquid is nonwetting, the liquid-solid interfacial energy is reduced by $\Delta\gamma A_{GS}$, where $\Delta\gamma$ is the difference between the gas-solid and liquid-solid interfacial energy, and $A_{GS} = 2\pi rh$ is the gas-solid interface area. Note that, if the effective gas-liquid interfaces are irregular, geometry factors should be used in the calculations of A_{GL} and V_G, which are ignored in the following discussion for the sake of simplicity.

The thermodynamics equilibrium condition can then be stated as

$$\Delta\mu \cdot V_G + \gamma_{GL} \cdot A_{GL} + p \cdot \Delta V = \Delta\gamma A_{GS}, \tag{1}$$

which can be rewritten as

$$r = r_{cr} \tag{2}$$

or

$$h = h_{cr} \tag{3}$$

where $r_{cr} = \dfrac{2\Delta\gamma}{(p+\Delta\mu) + 2\gamma_{GL}/h}$ is the critical pore radius and $h_{cr} = \dfrac{2\gamma_{GL}}{2\Delta\gamma/r - (p+\Delta\mu)}$ is the critical nucleus size of gas phase. According to Eq.(2), when $r < r_{cr}$, the gas phase is stable and can expand spontaneously, which eventually leads to the "outflow"; when $r > r_{cr}$, the liquid-to-gas phase transformation is energetically unfavorable and therefore the gas phase nucleus will vanish, resulting in the "nonoutflow". The relationship between r_{cr} and h is shown in Fig.3. The value of $\Delta\gamma$ is estimated as $p_{in}\bar{r}/2$, and $\Delta\mu$ is taken as $\mu_0 \cdot \rho_G$, where $\mu_0 = 2257.1$ J/kg is the specific energy of evaporation of water and ρ_G is the density of gas phase, which, if we assume that the gas phase follows the law of ideal gas, can be assessed as $\rho_G = \rho_0/(1+p/p_{at})$, with $\rho_0 = 1.21$ kg/m^3 being the air density at p_{at}. For the first-order approximation, the macroscopic value of γ_{GL}, 72 mJ/m^2, is used. Figure 3 indicates that decreasing p or increasing h is beneficial to keeping $r < r_{cr}$. According to Eq.(3), there exists an ultimate pore size $r_{ul} = \dfrac{2\Delta\gamma}{p+\Delta\mu}$, at which $h_{cr} \to \infty$. If $r > r_{ul}$, the "outflow" is impossible for any $\{\Delta\gamma, \Delta\mu, \gamma_{GL}, p\}$.

Based on a Fourier Transform Infrared Spectroscopy (FTIR) analysis, it was confirmed that, at liquid-solid interfaces, there exist a large number of nm-scale gas phase nuclei.[11] As temperature rises, the fraction of bigger nuclei increases, i.e. the average h is larger, which explains that, under p_{at}, while at room temperature the "outflow" was negligible, when $T > 50$°C the gas phase nucleation and growth could

occur. After the room-temperature resting, however, due to the significant decrease in gas content in the nanopores, the average size of gas phase nuclei is smaller, and therefore the same thermal treatment can cause only a reduced system recovery.

Future Work

The proposed research and work plan are not affected by the transfer of the place of operation. The objective of the proposed research program is to provide a scientific basis for the development of high-performance nanoporous volume-memory systems that are of superior energy density and deformability. The effects of admixtures, surface properties, porous structures, temperature, and potential difference on the solid-liquid interfacial energy and the kinetics of infiltration will be investigated systematically through experiments and computer simulations.

In the first period, we will focus on:
(1) Understanding the behaviors of nanoporous carbon based systems through infiltration measurements. Nanoporous carbon particles and membranes with various pore sizes and pore volume fractions will be tested.
(2) Performing infiltration experiment on nanoporous zeolite and silica based systems at various temperatures, through which the thermal effect can be analyzed.
(3) Performing staged infiltration experiment on nanoporous systems to analyze the kinetics of infiltration under various conditions.

In the second period, based on the experimental results obtained in year 1, we will further investigate the nanoporous intelligent systems:
(1) Continue the infiltration experiment on nanoporous systems to evaluate different surface treatment techniques and admixtures.
(2) Continue the staged infiltration experiment to analyze the "flow" rate in nanopores, with the pore size and surface species varying in broad ranges. The effects of the properties of gas species will be investigated.
(3) Evaluate the effectiveness of intrinsic and extrinsic factors through atomic simulations. The results will be compared with the experimental data.
(4) Perform numerical analyses on the evolution of effective pore clusters, such that the atomic behaviors in nanopores can be related to the aggregate response of nanoporous particles.

In the third period, with the important factors being fundamentally much better understood, the study will lead to the eventual optimization of the systems:
(1) Complete the experiment on intelligent systems of different admixtures and surface properties.
(2) Develop the multiscale model.
(3) Complete the parameterized study and identify the optimum materials and processing conditions.
(4) If necessary, investigate nanoporous systems based on metal doped zeolites so as to control the conductivity of electrodes.
(5) Complete reporting of experimental and simulation results.

Table I. The system recoverability, $R_s = \dot{E}_2/\dot{E}_1$, as a function of the thermal treatment temperature, T, where $\dot{E}_i$ is the absorbed energy in the i-th loading-unloading cycle ($i = 1,2$).

T (°C)	21	30	40	50	70	80
R_s (%)	11.3	24.4	45.0	94.3	97.4	97.0

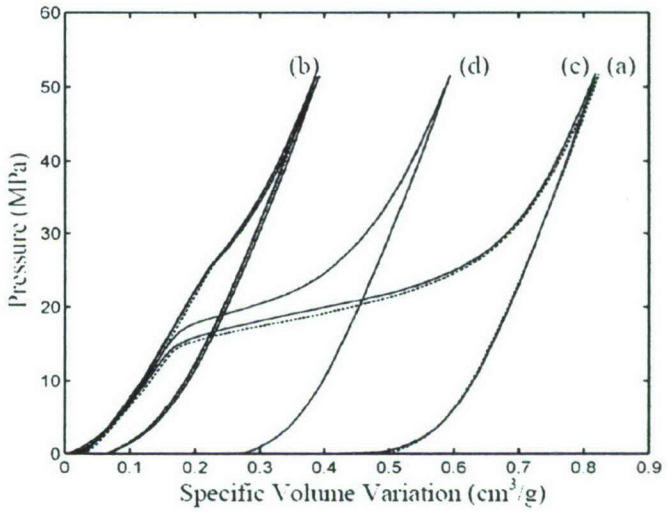

Fig.1 The sorption isotherm curves: (a) the first loading-unloading cycle (the dashed line); (b) the second (the dotted line), the third, and the fourth loading-unloading cycles without thermal treatment; (c) after the immediate thermal treatment; and (d) after the postponed thermal treatment.

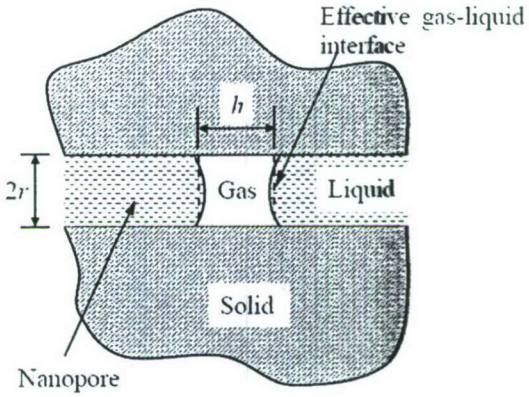

Fig.2 A schematic diagram of the confined phase transformation in a nanopore.

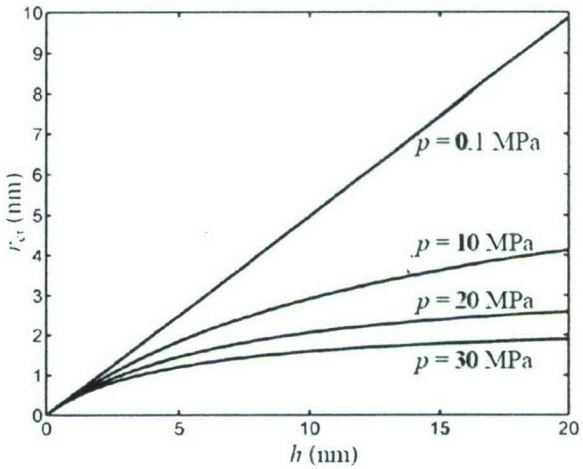

Fig.3 The relationship between r_{cr} and h.